Effects of Damping and Varying Contact Area at Blade-Disk Joints in Forced Response Analysis of Bladed Disk Assemblies

E. P. Petrov

D. J. Ewins

Centre of Vibration Engineering,
Mechanical Engineering Department,
Imperial College London,
South Kensington Campus,
London SW7 2AZ, UK

An approach is developed to analyze the multiharmonic forced response of large-scale finite element models of bladed disks taking account of the nonlinear forces acting at the contact interfaces of blade roots. Area contact interaction is modeled by area friction contact elements which allow for friction stresses under variable normal load, unilateral contacts, clearances, and interferences. Examples of application of the new approach to the analysis of root damping and forced response levels are given and numerical investigations of effects of contact conditions at root joints and excitation levels are explored for practical bladed disks. [DOI: 10.1115/1.2181998]

1 Introduction

Bladed disks are subjected to high levels of vibration amplitudes excited under service conditions by aerodynamics forces. Such forces can have a very dense frequency spectrum and, similarly, the spectrum of the natural frequencies of practical structures is also customarily very dense. These dense excitation and natural frequency spectra combine to make the task of avoiding all resonance regimes almost impossible. Because of that the problem of developing methods in order to provide accurate, fast, and robust predictive tools for the analysis of forced vibration response levels of bladed disks under operating conditions is a problem of major practical importance.

Accuracy of prediction of forced response levels is dependent on the modelling of bladed disk components (i.e., blades, disk, shroud, damping devices, etc.) and on the modeling of the interaction forces at the contact interfaces between these components.

Demands made by the gas-turbine industry to increase the accuracy of predictive analysis methods for forced response of bladed disks require development of advanced models and methods describing in detail all components of the bladed disk including the interaction of these components at the joints of the assembly. Friction at blade-disk joints is an important source of damping in bladed disk assemblies. It results from the action of friction forces caused by usually small relative motions between blades and the disk at the contacting surfaces of the blade roots. The contact interaction forces have a strongly nonlinear character due to: (i) slip-stick transitions, (ii) the unilateral character of the interaction force acting along a normal to the contact surface, (iii) the influence of normal force on slip-stick transitions and the magnitude of the friction force, (iv) variation of contact area where slip occurs during each cycle of vibration, and others.

Moreover, variation of the contact area at the blade roots induced by the blade vibration also causes variation of the elasticity and stiffness properties of blade-disk joints over each vibration cycle and hence can affect resonance frequencies of a bladed disk.

Methods for forced response analysis of bladed disk assemblies must allow calculations to be performed which include all these nonlinear effects, i.e., they are to be representative.

Bladed disks are structures of complex geometric shape and dynamical properties. Numerical analysis of forced response levels of bladed disks commonly requires the application of detailed finite element (FE) models in order to describe realistic design features and to achieve practically acceptable accuracy. The number of degrees of freedom in realistic finite element models can reach 10^5–10^7 (see, for example, Ref. [13]) which makes the numerical cost of forced response calculations large, even in linear forced response calculations. For the case of bladed disks with friction contacts at the blade roots, a nonlinear vibration analysis is essential. The nonlinear forced response analysis requires solution of nonlinear equations of motion, which is much numerically more expensive than the conventional analysis methods used for linear vibrations. Because of this, special reduction techniques are necessary to make the use of large-scale models feasible in the analysis of nonlinear vibrations of bladed disks.

There are several reported theoretical and experiments studies of blade-disk joints (see, e.g., Refs. [1–4]) where static loading and deformations are considered. These studies are focused mostly on the analysis of contact stresses and stresses in areas close to the contact interfaces. Detailed FE models are often developed only for small areas adjacent to the contact interface itself to make the calculations feasible and cost effective. Solutions of nonlinear dynamic problems in bladed disks (see Refs. [5–14]) have been performed for localized contacts in special devices, such as friction dampers, or for localized contacts of blade shrouds. The main problem for the dynamic analysis of bladed disks with root joints, and the effects of root damping, on forced response of bladed disks has not been investigated to date.

In this paper, a new method for the analysis of nonlinear forced response of bladed disks with blade-disk joints in frequency domain is proposed. Special friction area contact elements are developed to the model nonlinear interaction phenomena which occur at the friction contact interfaces in the blade roots. These contact elements take account of any time variation of the actual contact area during vibration, the unilateral character of interaction of mating surfaces along normal direction to the contact interface and the stick-slip transitions for friction contacts. Large-scale FE models describing design features in detail are implemented. The method includes the multiharmonic balance formulation of the equations of motion for steady response and a technique developed for efficient reduction of the number of degrees of freedom in resolving nonlinear equations which preserves the necessary accuracy and completeness of the initial large scale finite element models. Numerical investigations of multiharmonic

Contributed by the International Gas Turbine Institute (IGTI) of ASME for publication in the JOURNAL OF TURBOMACHINERY. Manuscript received August 25, 2005; final manuscript received September 28, 2005. IGTI Review Chair: K. C. Hall. Paper presented at the ASME Turbo Expo 2005: Land, Sea, and Air, Reno, NV, June 6–9, 2005, Paper No. GT2005-68936.

 Copyright © 2006 by ASME

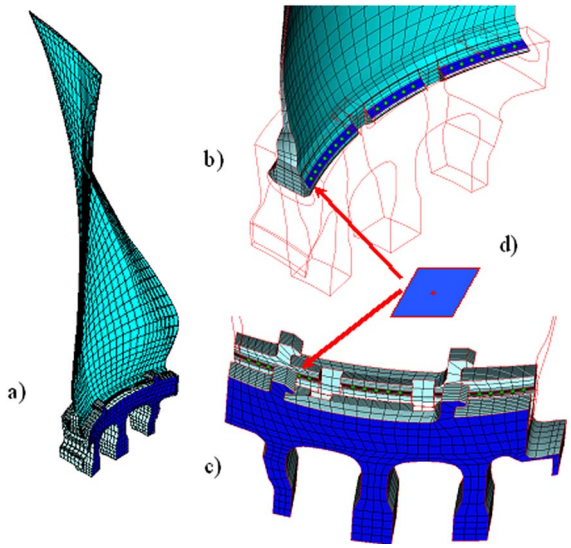

Fig. 1 Bladed disk models: (*a*) a bladed disk sector; (*b*) master nodes of the reduced model at blade contact surfaces; (*c*) master nodes at disk contact surfaces; and (*d*) an area contact element

forced response accounting for nonlinear interactions at blade-disk joints are performed for the first time for realistic bladed disks.

2 A Method for the Predictive Forced Response Analysis of Bladed Disks With Root Joints

The equation for motion for a bladed disk (see Fig. 1, where one sector of a bladed disk is shown) with friction contact interfaces can be written in the following form:

$$\mathbf{K}_\Sigma \mathbf{q}_\Sigma + \mathbf{C}_\Sigma \dot{\mathbf{q}}_\Sigma + \mathbf{M}_\Sigma \ddot{\mathbf{q}}_\Sigma + \mathbf{f}_\Sigma(\mathbf{q}_\Sigma) = \mathbf{p}_\Sigma(t) \tag{1}$$

where $\mathbf{q}_\Sigma(t)$ is a vector of displacements for all degrees of freedom (DOFs) in the structure considered; $\mathbf{K}_\Sigma$, $\mathbf{C}_\Sigma$, and $\mathbf{M}_\Sigma$ are stiffness, viscous damping, and mass FE matrices used for description of linear forces; $\mathbf{f}_\Sigma(\mathbf{q})$ is a vector of nonlinear interface forces, which is dependent on displacements DOFs at interface nodes; and $\mathbf{p}_\Sigma(t)$ is a vector of excitation forces. Thus, the problem of modeling bladed disks with friction interfaces at the blade roots can be separated into three major parts: (i) modeling of the bladed disk assembly, or its components, when only linear forces are allowed for (i.e., constructing matrices $\mathbf{K}_\Sigma$, $\mathbf{C}_\Sigma$, and $\mathbf{M}_\Sigma$); (ii) modelling of the friction contact interaction at the root contact surfaces (calculation of $\mathbf{f}_\Sigma(\mathbf{q})$), and (iii) combining the models for the bladed disk and the contact interfaces. Approaches developed to resolve these issues in the analysis of bladed disks with friction interaction at blade roots are discussed in this section together with a multiharmonic formulation of the equation of motion and a method for calculation of the amplitudes of vibration.

2.1 Models for Blades and a Disk. Models for bladed disks with linear forces only allowed for are constructed using the finite element method. This is now a well-established method widely used in practice in the gas-turbine industry. Commercial FE software packages available allow stiffness and mass matrices to be routinely calculated for large-scale FE models. A specific feature necessary for the FE models created for the analysis of bladed disks with friction contact interfaces require introduction mating nodes at all contact surfaces where nonlinear contact interaction can be expected. These mating nodes can have the same spatial coordinates, but the stiffness, $\mathbf{K}_\Sigma$, and mass, $\mathbf{M}_\Sigma$, matrices of the FE model for the bladed disk are calculated assuming that these nodes are disconnected and, hence, that all contact surfaces are free. The total number of degrees of freedom, N, in a large-scale FE bladed disk model is usually too large to permit nonlinear forced response calculations to be made using the matrices $\mathbf{K}_\Sigma$ and $\mathbf{M}_\Sigma$ directly. In order to make use of these models in nonlinear forced response analysis to be feasible, we apply the modal synthesis method developed in Ref. [15] and which can efficiently reduce the size of large FE models. To do this reduction, all DOFs of a bladed disk, $\mathbf{q}_\Sigma$, can be expressed through a selected subset of DOFs—so-called "master" DOFs, $\mathbf{q}^m$, and special modal DOFs, ξ, in the following way:

$$\underset{N\times 1}{\mathbf{q}_\Sigma} = \begin{Bmatrix} \mathbf{q}^m \\ \mathbf{q}^S \end{Bmatrix}_{N\times 1} = \underset{N\times n}{\begin{bmatrix} \mathbf{I} & \mathbf{0} \\ \mathbf{B} & \mathbf{\Phi} \end{bmatrix}} \underset{n\times 1}{\begin{Bmatrix} \mathbf{q}^m \\ \xi \end{Bmatrix}} = \underset{N\times n}{\mathbf{T}} \underset{n\times 1}{\begin{Bmatrix} \mathbf{q}^m \\ \xi \end{Bmatrix}} \tag{2}$$

Here, $\mathbf{q}^S$ is a vector of so-called "slave" DOFs, which are eliminated after reduction; and $\mathbf{I}(n\times n)$ is the identity matrix. The number, n, of DOFs retained in the reduced model, $\mathbf{q}=\{\mathbf{q}^m, \xi\}^T$, can be much smaller than total number of DOFs in the original structure, N, i.e., $n=size(\mathbf{q}^m)+size(\xi)\ll N$. Matrices $\mathbf{B}$ and $\mathbf{\Phi}$ used in Eq. (2) are determined from the solution of the following two conjugated problems:

1. Each jth column of matrix $\mathbf{B}$ is determined from a solution of the following static problem with respect to the vector of slave DOFs, $\mathbf{q}^S$:

$$\mathbf{K}_\Sigma \mathbf{q}_\Sigma = \mathbf{0} \tag{3}$$

when the corresponding master coordinate $\mathbf{q}_j^m=1$ and all the other master DOFs are zero.

2. The jth column of matrix $\mathbf{\Phi}$ is the jth mode shape obtained for vector of slave DOFs, $\mathbf{q}^S$, from solution of the following eigenproblem when all master DOFs are fixed (i.e., when $\mathbf{q}^m=\mathbf{0}$):

$$\mathbf{K}_\Sigma \mathbf{q}_\Sigma = \omega^2 \mathbf{M}_\Sigma \mathbf{q}_\Sigma \tag{4}$$

For analysis of variable contact and friction at root joints, master degrees of freedom are selected at the mating nodes of the blade root and disk contact surfaces. In addition, master nodes are also selected in the blade body to ensure acceptable accuracy of the dynamic model condensation. An example of master nodes used for forced response analysis of a bladed disk with friction at blade roots is shown in Fig. 1.

Substitution of Eq. (2) into Eq. (1) gives a reduced equation of motion for the bladed disk

$$\mathbf{K}\mathbf{q} + \mathbf{C}\dot{\mathbf{q}} + \mathbf{M}\ddot{\mathbf{q}} + \mathbf{f}(\mathbf{q}) = \mathbf{p}(t) \tag{5}$$

where $\mathbf{K}=\mathbf{T}^T\mathbf{K}_\Sigma\mathbf{T}$; $\mathbf{M}=\mathbf{T}^T\mathbf{M}_\Sigma\mathbf{T}$; $\mathbf{C}=\mathbf{T}^T\mathbf{C}_\Sigma\mathbf{T}$ and $\mathbf{p}=\mathbf{T}^T\mathbf{p}_\Sigma$. The ratio, n/N, of the number of DOFs before and after mode synthesis method reduction can take values of $10^{-2}-10^{-3}$.

2.2 Multiharmonic Balance Equation of Motion. Steady-state periodic regimes of vibration response are sought by making a transformation of the equation of motion (5) formulated in time domain into the frequency domain. In order to search for a periodic vibration response, the time variation of all DOFs of the system is represented as restricted Fourier series, which can contain as many and such harmonic components as are necessary to approximate the solution with a desired accuracy, i.e.

$$\mathbf{q}(t) = \mathbf{Q}_0 + \sum_{j=1}^{n} \mathbf{Q}_j^c \cos m_j\omega t + \mathbf{Q}_j^s \sin m_j\omega t \tag{6}$$

where n is the number of harmonics kept in the multiharmonic solution; $\mathbf{Q}_0$, $\mathbf{Q}_j^c$, and $\mathbf{Q}_j^s$ $(j=1,\ldots,n)$ are vectors of harmonic coefficients for the system DOFs; m_j $(j=1,\ldots,n)$ are the specific harmonics that are kept in the displacement expansion in addition to the constant component, and ω is the fundamental vibration frequency. In accordance with the multiharmonic balance method, the expansion from Eq. (6) is substituted into Eq. (5) which is sequentially multiplied by $(\cos m_j\omega)$ and $(\sin m_j\omega)$ and then integrated over the vibration period. As a result, equations for deter-

mining all the harmonic components are obtained in the following form:

$$\mathbf{R}(\mathbf{Q}) = \mathbf{Z}(\omega)\mathbf{Q} + \mathbf{F}(\mathbf{Q}) + \mathbf{P} = \mathbf{0} \tag{7}$$

where $\mathbf{Q}=\{\mathbf{Q}_0, \mathbf{Q}_1^c, \ldots, \mathbf{Q}_n^s\}^T$ is a vector containing all harmonic coefficients for displacement; $\mathbf{P}=\{\mathbf{P}_0, \mathbf{P}_1^c, \mathbf{P}_1^s, \ldots, \mathbf{P}_n^s\}^T$ is a vector of the harmonic coefficients of excitation forces, which for bladed disks are usually due to the aerodynamic forces caused by inhomogeneous gas flow and $\mathbf{F}(\mathbf{Q})=\{\mathbf{F}_0(\mathbf{Q}), \mathbf{F}_1^c(\mathbf{Q}), \ldots, \mathbf{F}_n^s(\mathbf{Q})\}^T$ is a vector of multiharmonic nonlinear friction contact forces acting at the blade-disk interfaces. The dynamic stiffness matrix involved in Eq. (7) has the form

$$\mathbf{Z}(\omega) = \begin{bmatrix} \mathbf{K} & \mathbf{0} & \mathbf{0} & \cdots & \mathbf{0} \\ \mathbf{0} & \mathbf{K}-(m_1\omega)^2\mathbf{M} & m_1\omega\mathbf{C} & \cdots & \mathbf{0} \\ \mathbf{0} & -m_1\omega\mathbf{C} & \mathbf{K}-(m_1\omega)^2\mathbf{M} & \cdots & \mathbf{0} \\ \cdots & \cdots & \cdots & \cdots & m_n\omega\mathbf{C} \\ \mathbf{0} & \mathbf{0} & \mathbf{0} & \cdots & \mathbf{K}-(m_n\omega)^2\mathbf{M} \end{bmatrix} \tag{8}$$

The multiharmonic balance formulation avoids the conventional time-consuming integration of equation. Instead, the nonlinear algebraic equation (7) is formed with respect to harmonic coefficients of displacement. The matrix of multiharmonic dynamic stiffnesses in Eq. (8) is formed from the stiffness, damping, and mass matrices of the linear part of the structure. Although it is quasi-diagonal, the matrix in Eq. (7) represents a simultaneous system of equations since coefficients for all harmonics are interdependent through a vector of multiharmonic nonlinear friction contact forces acting at blade-disk joints $\mathbf{F}(\mathbf{Q})=\{\mathbf{F}_0(\mathbf{Q}), \mathbf{F}_1^c(\mathbf{Q}), \ldots, \mathbf{F}_n^s(\mathbf{Q})\}^T$.

2.3 Solution of the Nonlinear Equations and Tracing of the Solution. Equation (7) represents a nonlinear set of equations with respect to $\mathbf{Q}$. One of the most efficient methods for solution of the nonlinear equations is the Newton–Raphson method, which possesses quadratic convergence when an approximation is close enough to the solution. An iterative solution process is expressed by the following formula:

$$\mathbf{Q}^{(k+1)} = \mathbf{Q}^{(k)} - \left(\frac{\partial \mathbf{R}^{(k)}}{\partial \mathbf{Q}}\right)^{-1} \mathbf{R}(\mathbf{Q}^{(k)}) \tag{9}$$

where superscript (k) indicates the number of the current iteration. By differentiating Eq. (8) with respect to $\mathbf{Q}$, a recurrence formula can be rewritten in the form

$$\mathbf{Q}^{(k+1)} = \mathbf{Q}^{(k)} - \left[\mathbf{Z}(\omega) + \frac{\partial \mathbf{F}(\mathbf{Q}^{(k)})}{\partial \mathbf{Q}}\right]^{-1} \mathbf{R}(\mathbf{Q}^{(k)}) \tag{10}$$

The matrix $\mathbf{Z}(\omega)$ is a multiharmonic dynamic stiffness matrix introduced in Eq. (7). A matrix of derivatives, $\mathbf{K}_{\text{nln}}(\mathbf{Q}) = \partial \mathbf{F}(\mathbf{Q})/\partial \mathbf{Q}$, also called "a tangent stiffness matrix," describes the stiffness properties of the friction contact interfaces determined for a current vector of multiharmonic amplitudes, $\mathbf{Q}$. The vector of nonlinear friction contact forces acting at blade-disk joints $\mathbf{F}(\mathbf{Q})$ and the tangent stiffness matrix of the friction contact interface, $\mathbf{K}_{\text{nln}}(\mathbf{Q})$ fully describe interaction of bladed and disk at blade-disk joints and allows the nonlinear forced response to be determined.

2.4 Friction Contact Modeling: Area Contact Elements. Special friction area contact elements have been developed to model friction contacts of blade and disk at the blade root contact surfaces. The friction contact elements allow for variation of area of the contact patches during bladed disk vibration, friction stresses with effects of variable normal stresses on stick-slip transitions and friction stresses' levels. Moreover unilateral character of blade-disk interaction along normal to the contact surfaces can be described. This unilateral interaction occurs due to the fact that only compressing normal stresses can act at the contact surfaces but not the tensile stresses. Because of that when the mating contact surfaces are temporarily separated during vibrations the normal stresses become equal to zero and cannot take negative values. In order to model blade-disk interaction at the contact patches of the blade roots the area contact elements are distributed over the surfaces where nonlinear forces can be expected (as shown in Fig. 1(*d*)). The friction area contact element developed allows automatic determination of all possible contact interaction states for a small area covered by the contact element including stick, slip, and separation. Friction contact models for time-domain analysis were developed in paper [16] and friction contact elements for frequency-domain analysis were developed in paper [14].

Table 1 Stresses of the friction contact interaction

Status	Tangential force σ_t	Normal force σ_n
Contact Slip: $\xi\mu\sigma_n$	Stick: $k_t(u_t - u_t^{(0)}) - \xi\mu\sigma_n^{(0)}$	$\sigma_0 + k_n u_n$
Separation	0	0

The friction contact elements developed in paper [14] are extended here to modeling area contact for analysis of bladed disks with blade-disk contact interfaces. In contrast to paper [14], these friction area contact elements express contact stresses but not contact forces in terms of the relative displacements along a direction tangential to the contact surface, $u_x(\tau)$, and a normal relative displacement, $u_y(\tau)$. There are several major possible states of the contact interaction and expressions for tangential and normal components of the interaction force are shown for each of these in Table 1.

Here $u_t^{(0)}=u_t(\tau_{stick})$ and $\sigma_n^{(0)}=\sigma_n(\tau_{stick})$ are values of the tangential displacement and of the normal stresses at the beginning of the current stick state, τ_{stick}, and σ_0 is static normal stresses which are due to action of centrifugal, thermoelastic, and static aerodynamic forces. k_t and k_n are contact stiffness coefficients for tangential and normal deformations accordingly, and $\xi = \text{sgn}(\sigma_t(\tau_{slip})) = \pm 1$ is a sign function. Equations that are used to determine time instants when contact state changes are given in Table 2.

Since periodic steady-state vibrations are analyzed, the relative displacements, $x(\tau)$ and $y(\tau)$ can be expressed as a Fourier series with a restricted number of harmonics

$$u_t(\tau) = \mathbf{H}_-^T(\tau)\mathbf{X}; \quad u_n(\tau) = \mathbf{H}_-^T(\tau)\mathbf{Y} \tag{11}$$

where $\mathbf{H}_-=\{1, \cos m_1\tau, \sin m_1\tau, \ldots, \cos m_n\tau, \sin m_n\tau\}^T$; m_j are numbers of harmonics that are used in the multiharmonic expansion, and $\mathbf{X}$ and $\mathbf{Y}$ are vectors of harmonic coefficients of relative motion in the tangential and normal directions, respectively. The nondimensional time, $\tau=\omega t$, is introduced here using the principal frequency, ω, of the multiharmonic vibrations which defines period of the vibrations.

A method developed in Ref. [14] allows the exact determination of the contact stresses and tangent stiffness matrix of the friction contact interface as a function of relative displacements for a gen-

Table 2 Conditions of the friction contact state transition

Stick to slip	Slip to stick	Contact to separation
$\sigma_t(\tau) = \pm\mu\sigma_n(\tau)$ $\xi\dot{\sigma}_t < \mu\dot{\sigma}_n$	$\xi k_t \dot{u}_t(\tau) = \mu k_n \dot{u}_n(\tau)$ $\xi k_t \ddot{u}_t < \mu k_n \ddot{u}_n$	$\sigma_n = 0$ $\dot{u}_n < 0$

eral case of multiharmonic vibrations. In accordance with the method, the interaction stresses given in Table 1 are expanded into Fourier series

$$\sigma_t(\tau) = \mathbf{H}_-^T(\tau)\mathbf{S}_t(\mathbf{X},\mathbf{Y}); \quad \sigma_n(\tau) = \mathbf{H}_-^T(\tau)\mathbf{S}_n(\mathbf{Y}) \tag{12}$$

The vectors of multiharmonic components for tangential, $\mathbf{S}_t(\mathbf{X},\mathbf{Y})$, and normal, $\mathbf{S}_n(\mathbf{Y})$, stresses are obtained in an explicit form as functions of vectors of harmonic coefficients of relative motion along tangential and normal directions to the contact surface, $\mathbf{X}$ and $\mathbf{Y}$.

The contact area can be now covered by the area contact elements. These elements are usually chosen to be relatively small to allow distributions of the traction and normal stresses to be accurately interpolated over each of the elements. The values of the contact stresses are evaluated at a set of nodes usually located within and on boundaries of the area contact elements. For each node, the tangential friction forces and normal unilateral forces are calculated in the local coordinate system with axes directed along normal and tangential directions of the contact surface that are defined for a current point, xyz. The contact stresses in global coordinate system, $\overline{xyz}$, are then interpolated using the contact forces evaluated at several nodes of the contact element area in the form

$$\bar{\boldsymbol{\sigma}} = \sum_j^{n_{nodes}} \mathbf{N}_j(x,y)\mathbf{R}(x_j,y_j)\boldsymbol{\sigma}(x_j,y_j) = \sum_j^{n_{nodes}} \mathbf{N}_j(x,y)\bar{\boldsymbol{\sigma}}(x_j,y_j) \tag{13}$$

where $\bar{\boldsymbol{\sigma}}=\{\sigma_{\bar{x}},\sigma_{\bar{y}},\sigma_{\bar{z}}\}^T$ is a vector of contact stresses interpolated; $\boldsymbol{\sigma}(x_j,y_j)=\{\sigma_t,\sigma_n\}^T$ is a vector of contact stresses calculated at the jth point, (x_j,y_j); n_{nodes} is number of nodes for the area contact element; $\mathbf{R}(x_j,y_j)$ is the so-called "rotation" matrix describing rotation of for the local coordinate system with respect to a coordinate system which is global and used for analysis of the whole structure. $\mathbf{N}_j(x,y)$ are conventional shape functions used in isoparametric finite elements. The standard FE procedure for the reduction of the contact stress distribution to the nodes of the finite element mesh can be applied. This procedure is based on equality of works performed by the nodal forces and the stresses distributed over the area of the element, which gives the following expression for the nodal force:

$$\mathbf{f}_j = \int_A N_j(x,y)\bar{\boldsymbol{\sigma}}(x,y)dA = \mathbf{H}_-^T(\tau)\mathbf{F}_j \tag{14}$$

where $\mathbf{f}_j=\{f_x,f_y,f_z\}^T$ is a vector of nodal forces at the jth node of the area contact element and $\mathbf{F}_j=\{\mathbf{F}_x,\mathbf{F}_y,\mathbf{F}_z\}^T$ is a vector of harmonic coefficients for the jth nodal forces. From Eqs. (12), (13), and (14), we derive expressions for harmonic coefficients of nodal forces in the form

$$\mathbf{F}_j = \int_A N_j(x,y)\bar{\mathbf{S}}(x,y)dA \tag{15}$$

where $\bar{\mathbf{S}}=\{\bar{\mathbf{S}}_0,\bar{\mathbf{S}}_1^{(c)},\ldots,\bar{\mathbf{S}}_n^{(s)}\}$ is a vector of harmonic coefficients for $\bar{\boldsymbol{\sigma}}$.

For the simplest case of the area element with one node located in the middle of the area, the multiharmonic components of the nodal forces can be expressed in the form

$$\mathbf{F} = \begin{Bmatrix} \mathbf{F}_t \\ \mathbf{F}_n \end{Bmatrix} = A \begin{Bmatrix} \mathbf{S}_t(\mathbf{X},\mathbf{Y}) \\ \mathbf{S}_n(\mathbf{X},\mathbf{Y}) \end{Bmatrix} \tag{16}$$

where A is area covered by the eth contact element. The tangent stiffness matrix of this contact element is determined by differentiating Eq. (16) with respect to vectors $\mathbf{X}$ and $\mathbf{Y}$

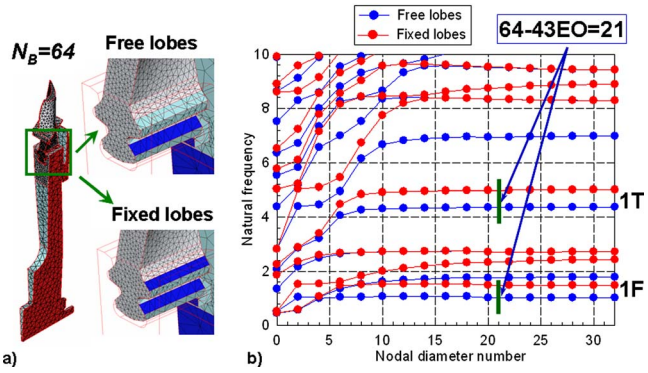

Fig. 2 Model (*a*), natural frequencies of the bladed disk with different contact conditions and frequency range of interest (*b*)

$$\mathbf{K}_e = \begin{bmatrix} \mathbf{K}_{tt} & \mathbf{K}_{tn} \\ \mathbf{0} & \mathbf{K}_{nn} \end{bmatrix} = \frac{\partial \mathbf{F}}{\partial\{\mathbf{X},\mathbf{Y}\}} = A \begin{bmatrix} \partial\mathbf{S}_t/\partial\mathbf{X} & \partial\mathbf{S}_t/\partial\mathbf{Y} \\ \mathbf{0} & \partial\mathbf{S}_n/\partial\mathbf{Y} \end{bmatrix} \tag{17}$$

Owing to analytical expressions obtained for $\mathbf{S}_t(\mathbf{X},\mathbf{Y})$ and $\mathbf{S}_n(\mathbf{Y})$ calculations of the tangent stiffness matrix for the contact interface can be made exactly and very fast. Further details of the contact force vectors and the stiffness matrix derivation can be found in Ref. [14]. Vectors of multiharmonic components of the contact forces, $\mathbf{F}_e$, and tangent stiffness matrices, $\mathbf{K}_e$, are calculated for all contact elements and added to the vector of nonlinear friction contact forces $\mathbf{F}(\mathbf{Q})$ and the tangent stiffness matrix of the friction contact interface, $\mathbf{K}_{\text{nln}}(\mathbf{Q})$.

3 Numerical Investigations

The method developed has been applied to analysis of realistic bladed turbine and fan bladed disks of gas-turbine engines. One of the considered test cases was a bladed turbine disk from a test rig of the EU-funded project ADTurb (see [17,18]). A sector of the FE model used in the analysis is shown in Fig. 2(*a*). The FE model is constructed using tetrahedral 10 node finite elements. The total number of blades in the bladed disk analyzed is 64. The number of DOFs in the FE model of one sector comprises 73,245 DOFs. Root damping is analyzed at contact surfaces of the first lobe of the two-lobe firtree blade root. First, a linear bladed disk model was analyzed. To assess a range of the possible variation of the resonance frequencies due to slip at blade root, the natural frequencies were calculated for two extreme cases: (i) a case when there is no contact between bladed and disk at the first lobe, and (ii) a case when all contact surfaces are fully stuck and slip does not occur. Due to confidentiality requirements, all frequencies in this paper are normalized by the first blade-alone resonance frequency and the forced response levels are also normalized. Calculated natural frequencies are shown for all possible nodal diameters numbers in Fig. 2(*b*). One can see that variation of the contact condition at the first lobe of the bladed disk can significantly affect the resonance frequencies.

The blade-disk interaction at the contact surfaces is essentially nonlinear since slip-stick or contact-separation transitions can occur at the contacting surfaces and, moreover, the contact area and contact conditions can vary during period of vibration. In order to predict forced response levels and damping caused by friction at the root contact surfaces the developed friction area contact elements are applied at the contact surfaces of interest. The FE model of the bladed disk is constructed for this purpose with the contact surfaces set to be free and the friction one-node area contact elements are distributed uniformly over these surfaces to describe nonlinear friction contact interaction between the blades and the disk. The reduced model obtained by application of the modal synthesis method has 332 DOFs. These DOFs includes 282 master DOFs (3 DOFs for each of 94 master nodes) and 50 modal coor-

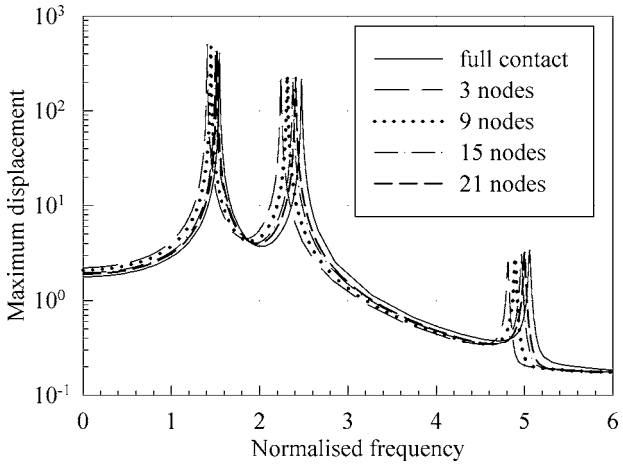

Fig. 3 Forces response of the bladed disk with stuck contact surfaces modeled by different number of the area contact elements

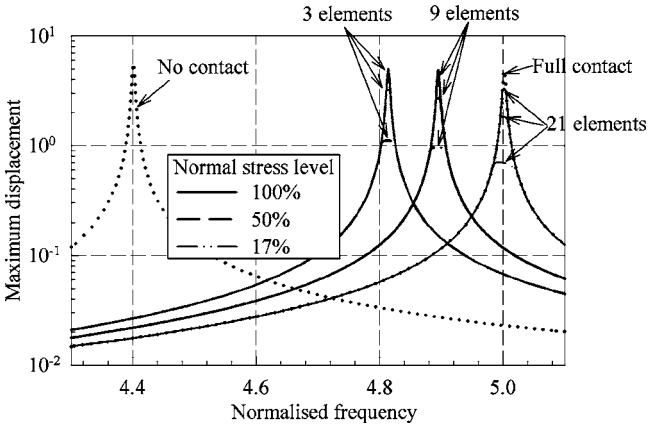

Fig. 5 The forced response levels for different levels of the static normal stresses and different numbers of the friction area elements applied at the contact surfaces

dinates. From 94 master nodes $4\times21=84$ are chosen on blade-disk mating contact surfaces at two contact patches of the blade root and are uniformly distributed over the contact surfaces. 10 master nodes are chosen at airfoil of the blade.

Damping loss factor, η, due to material and aerodynamic damping was assumed to be 0.001. Aerodynamic forces exciting the vibration analyzed were determined from aerodynamic calculations and are distributed over the blade airfoils. Excitation by 43th engine-order is considered which corresponds to a vibration mode of a tuned bladed disk with $64-43=21$ nodal diameters and frequency range corresponding to first flap-wise (1F) mode and first torsional (1T) mode are analyzed. A green line marks a frequency range for which the forced response analysis is performed. Friction coefficient at the contact surfaces was assumed to be 0.3. Total damping including effects of friction forces and variation of stiffness of the blade-disk joints due to variation of the contact areas and slip-stick transitions at the contact interfaces were determined in process of calculations by applied the friction area contact elements.

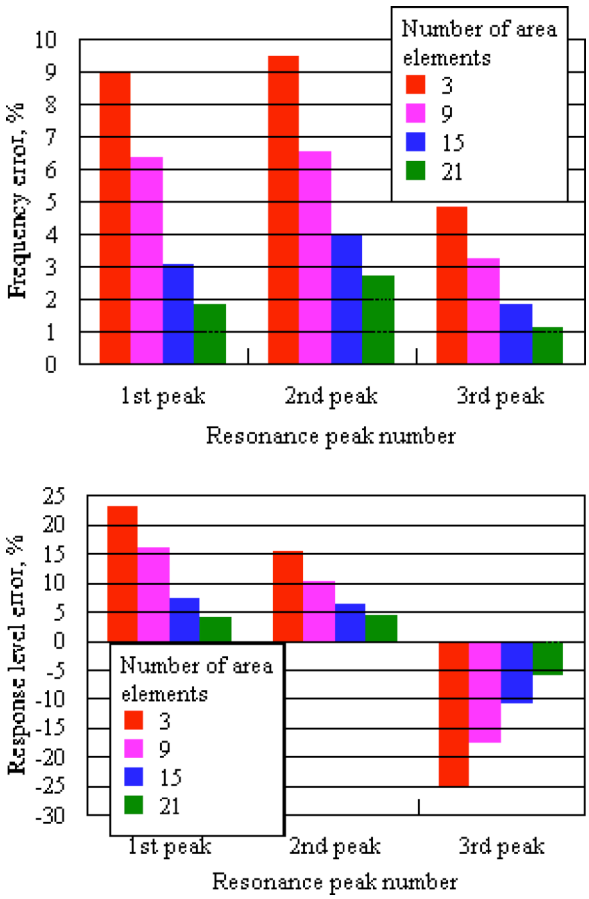

Fig. 4 Errors in prediction of the resonance characteristics for different number of the area contact elements: (*a*) For resonance frequencies and (*b*) for resonance amplitudes

The method developed reduces the number of DOFs in the whole structure to the number of degrees of DOFs where nonlinear contact forces are applied. Hence, the size of the resulting nonlinear equation is proportional to number of the friction contact elements applied to the bladed disk and, accordingly, the speed of calculations is dependent on number of these elements. In order to chose the number of contact elements providing acceptable accuracy for the area contact modeling together with high speed of calculation, an investigation of influence of the choice of number of the area elements on forces response levels and values of the resonance frequencies is performed. Four cases of (i) 3, (ii) 9, (iii) 15, and (iv) 21 one-node area contact elements applied over each of two (left and right) contact patches of the first lobe of the firtree root.

In each of the considered cases, the friction area contact elements cover the whole area of the contact patches; hence, area of contact represented by each element for these cases is 14.17, 4.73, 2.83, and 2.02 mm^2, accordingly. In order to explore the capability of the relative small number of the area contact elements to model a full stuck condition, the forced response was calculated with the large normal load excluding possibility of slip-stick transition at the contact patches. Since for this case the structure with friction contact elements exhibits linear behavior without friction damping, the forced response is compared with the forced response of linear structure determined for the FE model obtained for a case of fixed firtree lobes. Closeness of the resonance frequencies and amplitudes obtained for the model with the friction contact elements and from the FE model with fixed firtree lobes indicates accuracy of the contact modeling for a case of full contact. The calculated forced responses are compared in Fig. 3. This comparison is used to choose number of the area contact elements required in the analysis.

Errors in the prediction of the resonance frequencies and amplitudes are shown in Fig. 4. One can see that for the case of 21 area contact elements, for each of the two contact patches accept-

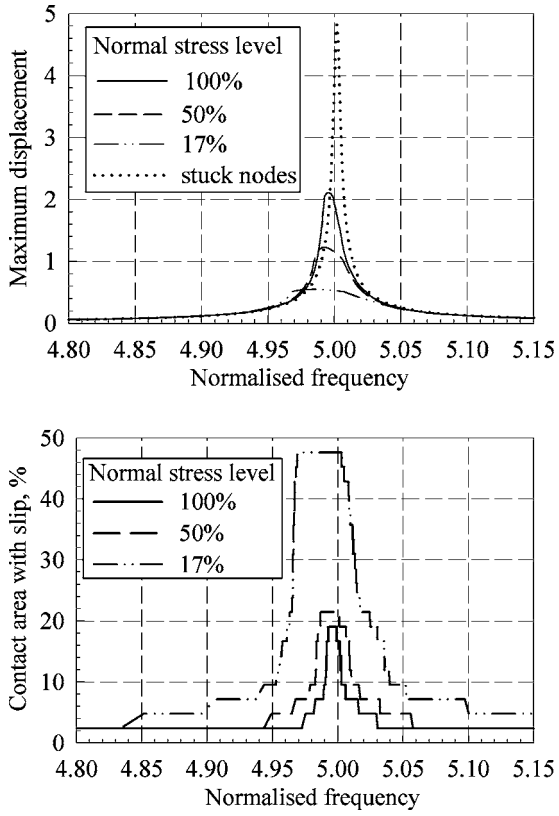

Fig. 6 Effects of different levels of the static normal stresses: (*a*) Forced response; and (*b*) contact area where slip occurs

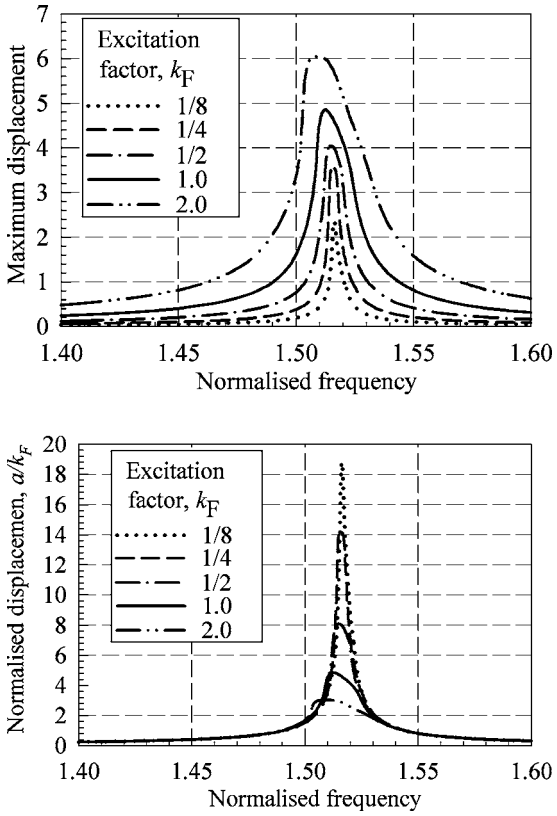

Fig. 8 Effects of the excitation level on the forced response in frequency range of 1F mode: (*a*) Displacement; and (*b*) displacement normalized by the excitation level

able accuracy is achieved for first 3 resonance frequencies (error $<2.7\%$) and resonance amplitudes (error $<5.8\%$).

Moreover, realistic normal stresses which are due to action of the centrifugal forces were calculated and then these static stresses are used in the forced response analysis for the area contact elements. Variation of the normal stresses over the contact patches is accounted for and hence different normal stress levels are applied to different area contact elements. Three different levels of the static normal stresses were studied, namely 100%, 50%, and 17% of the maximum level. These static stress levels occur in the bladed disk analyzed at rotation speeds: 100%, 70%, and 40% of the maximum rotation speed, respectively.

Results of calculation of the forced response levels for cases of 3 different levels of the normal stresses and for 3 cases of the number of the friction contact element applied over each contact patch are shown in Fig. 5. For comparison, forced responses calculated for two linear systems are also plotted there: (i) the forced response for a case when there is no contact with the disk at the first lobe of the blade root; and (ii) the forced response for a case when there is full contact at blade-disk joints and slip does not occur. One can see that there is more than an 8% shift in the resonance frequency between these two extreme linear cases. When 21 friction contact elements are applied at each contact, surface forced response level outside the vicinity of the resonance frequency is practically coinciding with that of the linear system with full contact. For these frequencies, the level of relative displacements is too small to cause slip at the contact interfaces or variation of the contact area. The resonance frequency for 100% level of the static normal stresses is very close to resonance frequency of this linear system. For cases of 3 and 9 friction contact elements per contact surface, there is a difference, although small, in resonance frequencies, which is due to a decrease in stiffness of the blade-disk joints when too small a number of the contact elements is used for contact modeling. In all of the following figures, results obtained with 21 friction contact elements at each of the contact surfaces are shown.

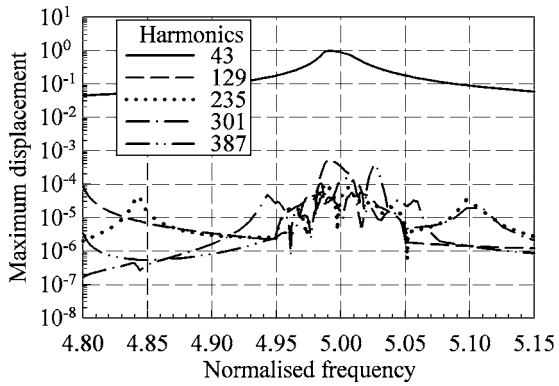

Fig. 7 Harmonic components for the multiharmonic forced response (calculated for the case of 50% of the normal stress level)

The effect of the level of the static normal stresses on levels of forced response is demonstrated in Fig. 6(*a*) for excitation frequencies in the range of 4.8–5.15 corresponding to 1T mode. The forced response of the linear system with full contacts is shown here for comparison.

The method allows determination of not only the forced response but also contact conditions at each point of the over area covered by the friction contact elements, including occurrence slipping parts. The size of the contact area where slip occurs related to the whole size of the contact patches is shown Fig. 6(*b*). One can see that the resonance frequency is not significantly af-

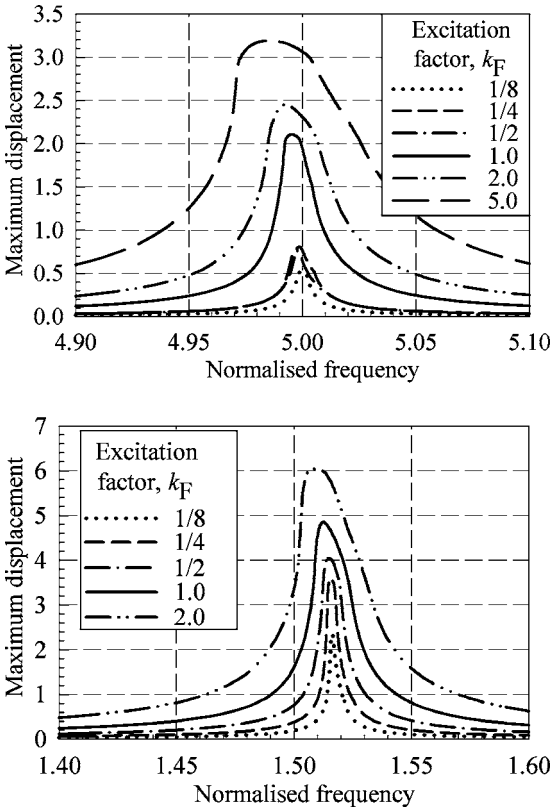

Fig. 9 Effects of the excitation level on the forced response in frequency range of 1T mode: (*a*) Displacement; and (*b*) displacement normalised by the excitation level

fected by the level of normal stresses and accordingly by effects of number of slipping nodes at the contact surface. Yet, the level of forced response is very sensitive to the normal stress level since the size of the contact area is involved in slip-stick transitions, and, therefore, the vibration energy is dissipated by the friction forces at these parts of the contact area. For the case considered, accounting for root damping reduces resonance amplitude in 2.5 times for 100% level of the normal stresses and in 10 times for 17% level. For the resonance frequency, 18% (for 100% normal stress level) and 22% (for 50% normal stress level) and 48% (for 17% normal stress level) of the whole contact area is subjected to slip at least over small time interval.

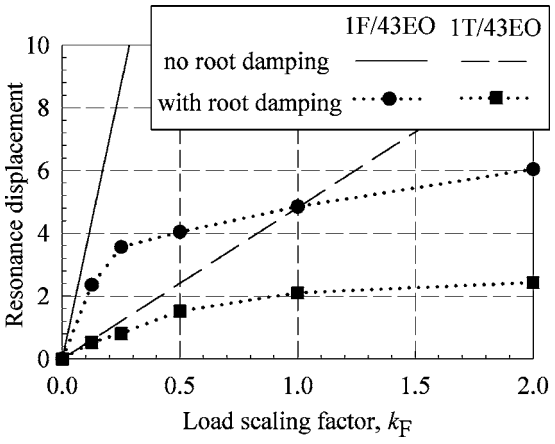

Fig. 10 Effects of the excitation level on the resonance displacement

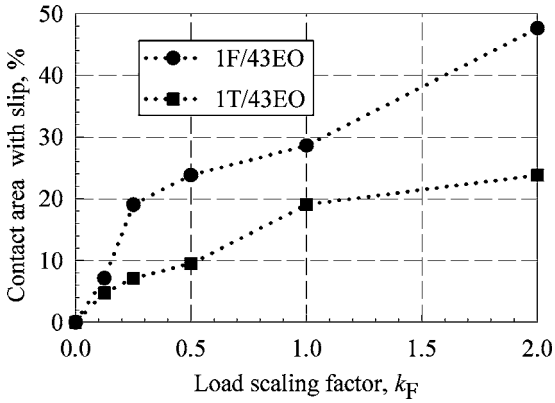

Fig. 11 Effects of the excitation level on the slipping area at resonance frequency

It is also important to note that although the friction forces produce strongly nonlinear blade-disk interaction at root joints, the harmonic coefficients of the multiharmonic forced response were small for all harmonics except of that coinciding with excitation harmonic. In the calculations, the first 6 odd multiplies from 1 to 9 of the excitation harmonic, 43EO are kept. An example of the amplitudes for all these harmonics in the multiharmonic expansion for displacement is shown in Fig. 7. One can see that the 43rd harmonic is predominant in the forced response and contribution of all the other can be neglected.

The effect of the excitation level on the response level is demonstrated in Fig. 8 for a frequency range including 1F mode, and in Fig. 9 for a frequency range including 1T mode. Distribution of the excitation loads over the blade airfoil in all cases was the same, but these loads were multiplied by a factor k_F with values from 1/8 to 5. In Figs. 8(*a*) and 9(*a*), the amplitude of the displacement is plotted. One can see that shape of the forced response curves significantly differs for the different levels of excitation. In Figs. 8(*b*) and 9(*b*), in order to clearly demonstrate the nonlinear dependency of this amplitude to excitation levels, it is normalized by dividing by k_F. For the case of the linear structure, the displacement normalized by k_F would be identical for all forced response levels, but they differ here and the highest level of excitation produces the smallest value of the normalized forced response. This is because at higher levels of vibration the larger part of the contact area starts slipping and therefore friction damping increases.

The resonance amplitude level as a function of level of excitation is plotted in Fig. 10 for both resonance modes analyzed: 1F and 1T. These functions have essentially nonlinear character. For comparison, straight lines show the resonance amplitudes that

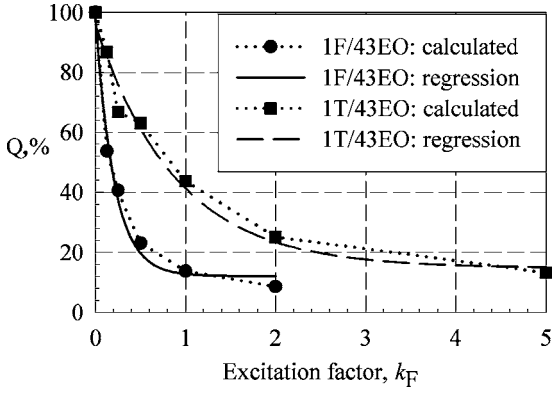

Fig. 12 Dependency of the *Q*-factor on the excitation level

Table 3 Approximation for the *Q*-factor as a function of the excitation level

Approximation coefficient	Mode	
	1F	1T
c_0	12.18	14.75
c_1	86.04	81.28
c_2	0.486	0.112

would realize if there were no friction damping at the blade root. Relative size of the slipping part of the contact area is shown in Fig. 11 for both resonating modes.

The calculations performed allow the determination of the damping in the structure caused by friction at blade root joints. The characteristics of the total damping in the structure, $Q=1/\eta$ (η is the total damping loss factor) were obtained directly from the calculated forced response functions in vicinity of the resonance frequency. The Q-factor extracted from results of the forced response is plotted as a function of excitation level in Fig. 12. The regression analysis was made for the calculated function and it was found that the three-parameter exponential function $Q=c_0+c_1e^{-c_2k_F}$ with values for the coefficient values given in Table 3 provides a good approximation for the Q-factor as a function of the excitation level.

4 Conclusions

An effective method for predictive analysis of inherent damping at blade-disk root joints has been developed. The method can use large-scale models for bladed disks with variable contact and friction at root joints. In order to achieve high speed of calculation, the multiharmonic balance formulation for nonlinear equation of motion is used. The formulation allows accuracy required to be achieved by keeping necessary number of harmonics in the solution and by choosing those harmonic number that are needed to approximate the solution sought.

The method is based on analytical formulation of friction area contact elements which allows exact calculation of multiharmonic components of interaction forces and of the tangent stiffness matrix of the joints for friction contact. Reduction in size of the model is performed by application of the modal synthesis method.

Acknowledgment

The authors are grateful to Rolls-Royce plc. for providing the financial support for this project and for giving permission to publish this work. The FE model used for the test case is based on the results of the European Community project ADTurB (Project BRPR-CT95-0124). Further details can be found at www.cordis.lu.

References

[1] Kenny, B., Patterson, E. A., Said, M., and Aradhya, K. S. S., 1991, "Contact Stress Distributions in a Turbine Disk Dovetail Type Joint—A Comparison of Photoelastic and Finite Element Results," Strain J. Brit. Soc. Strain Measurement, **27**, pp. 21–24.

[2] Meguid, S. A., Refaat, M. H., and Papanikos, P., 1996, "Theoretical and Experimental Studies of Structural Integrity of Dovetail Joints in Aeroengine Disks," J. Mater. Process. Technol., **56**, pp. 668–677.

[3] Papanikos, P., Meguid, S. A., and Stjepanovic, Z., 1998, "Three-Dimensional Nonlinear Finite Element Analysis of Dovetail Joints in Aeroengine Disks," Finite Elem. Anal. Design, **29**, pp. 173–186.

[4] Sinclair, G. B., Cormier, N. G., Griffin, J. H., and Meda, G., 2002, "Contract Stresses in Dovetail Attachments: I—Finite Element Modeling," Trans. ASME: J. Eng. Gas Turbines Power, **124**, pp. 182–189.

[5] Pierre, C., Ferri, A. A., and Dowell, E. H., 1985, "Multiharmonic Analysis of Dry Friction Damped Systems Using an Incremental Harmonic Balance Method," Trans. ASME, J. Appl. Mech., **52**, pp. 958–964.

[6] Wang, J. H., and Chen, W. K., 1993, "Investigation of the Vibration of a Blade With Friction Damper by HBM," Trans. ASME: J. Eng. Gas Turbines Power, **115**, pp. 294–299.

[7] Yang, B.-D., and Menq, C.-H., 1997, "Modelling of Friction Contact and its Application to the Design of Shroud Contact," Trans. ASME: J. Eng. Gas Turbines Power, **119**, pp. 958–963.

[8] Sanliturk, K. Y., Imregun, M., and Ewins, D. J., 1997, "Harmonic Balance Vibration Analysis of Turbine Blades With Friction Dampers," Trans. ASME, J. Vib. Acoust., **119**, pp. 96–103.

[9] Berthillier, M., Dupont, C., Mondal, R., and Barrau, R. R., 1998, "Blades Forced Response Analysis With Friction Dampers," Trans. ASME, J. Vib. Acoust., **120**, pp. 468–474.

[10] Szwedowicz, J., Sextro, W., Visser, R., and Masserey, P., 2003, "On Forced Vibration of Shrouded Turbine Blades," ASME Paper No. GT-2003-38808.

[11] Petrov, E. P., 2004, "A Method for Use of Cyclic Symmetry Properties in Analysis of Nonlinear Multiharmonic Vibrations of Bladed Disks," ASME J. Turbomach., **126**, pp. 175–183.

[12] Nacivet, S., Pierre, C., Thouverez, F., and Jezequel, L., 2003, "A Dynamic Lagrangian Frequency-Time Method for the Vibration of Dry-Friction-Damped Systems," J. Sound Vib., **265**, pp. 201–219.

[13] Petrov, E. P., and Ewins, D. J., 2004, "Method for Analysis of Nonlinear Multiharmonic Vibration of Bladed Disks Mistuned by Scatters in Characteristics of Friction Contact Interfaces and Blades," ASME Paper No. GT2004-53891.

[14] Petrov, E. P., and Ewins, D. J., 2003, "Analytical Formulation of Friction Interface Elements for Analysis of Nonlinear Multiharmonic Vibrations of Bladed Disks," ASME J. Turbomach., **125**, pp. 364–371.

[15] Craig, R. R., Jr., and Bampton, M. C. C., 1968, "Coupling of Substructures for Dynamic Analysis," AIAA J., **6**(7), pp. 1313–1319.

[16] Petrov, E. P., and Ewins, D. J., 2004, "Generic Friction Models for Time-Domain Vibration Analysis of Bladed Disks," ASME J. Turbomach., **126**, pp. 184–192.

[17] Green, J. S., 2001, "An Overview of a European Collaborative Programme for Forced Response," 6th National Turbine Engine High Cycle Fatigue Conference, Jacksonville, FL.

[18] Aeromechanical Design of Turbine Blades (ADTurB), Project funded by the European Community under the Industrial and Material Technologies Programme (Brite-EuRam III), Contract number: BRPR-CT95-0124, ADTurB Synthesis Report, 2001, 17 pp.